Observations of thermal diffusivity and a relation to the porosity of tidal flat sediments

Jim Thomson[1]

Received 6 November 2009; revised 22 December 2009; accepted 29 December 2009; published 19 May 2010.

[1] Time series observations of vertical profiles of sediment temperature are presented for several locations at two distinct tidal flats. Surface sediment temperatures are shown to be strongly dependent on solar insolation during low-tide exposure, and that signal is communicated to the subsurface sediment temperatures. A vertical diffusion balance explains the observations well (up to 97% of the observed variance at some locations and 76% on average), and an estimate of thermal diffusivity is obtained for each location. A theoretical model relating sediment porosity to thermal diffusivity is presented and shown to agree with independent estimates of porosity. In addition, thermal diffusivity is shown to correlate with direct observations of sediment composition (percent sand) and surface strength. Results are suggested for application to remote classification of sediments using infrared time series images.

Citation: Thomson, J. (2010), Observations of thermal diffusivity and a relation to the porosity of tidal flat sediments, *J. Geophys. Res.*, *115*, C05016, doi:10.1029/2009JC005968.

1. Introduction

[2] Tidal flats are regions of tactical and economic significance, yet quantification of sediment properties in these regions remains limited. Thermal properties are of particular significance, as intertidal sediments can absorb and store large quantities of heat [*Kim et al.*, 2007]. The heat content affects benthic habitats, for example the photosynthetic capacity of benthic microalgae [*Guarini et al.*, 1997]. In addition, the biology can affect the heat content, as in the ventilation of mud flats by manicure crabs [*Kim et al.*, 2009]. The large quantities of heat also have potential feedbacks on hydrodynamics via exchange with tide waters [*Cho et al.*, 2005]. This study evaluates thermal properties as a proxy for the porosity, or water content, of intertidal sediments, because of the strong difference in thermal characteristics between water and solid minerals [*Lovell*, 1985].

[3] Extending from the work of *Kim et al.* [2007], observations show evidence of thermal diffusion within intertidal sediments. A novel relation to sediment porosity is presented and then validated, based on two existing models relating the thermal properties of sediment to water content. In combining these models, the underlying argument is that the relative volume of water sets the net thermal response of the sediment-water mixture. This novel approach is motivated by the possibility of surveying sediments remotely using infrared sensing, since tidal flats are difficult to sample directly. Progress relating thermal properties to sediment composition will advance understanding towards infrared sensing of tidal flats, and, eventually, remote sediment classification.

[4] The *Lovell* [1985] model is the result of laboratory experiments which concluded that the thermal conductivity of marine sediments is well described by a geometric combination using the conductivity of water and the conductivity of solid quartz mineral. The model has been successfully used to determine the sound speed profile in natural marine sediments [*Jackson and Richardson*, 2002; *Subramaniam and Frisk*, 1992]. The *Campbell and Norman* [1998] model for the volumetric heat capacity of marine sediments uses the weighted sum of the heat capacities of the soil constituents. Combined, these models describe the thermal diffusivity of the sediments as function of porosity.

[5] First, observations are presented, and then the models used for analysis are described. Results are presented next, including validation of the novel relation between thermal diffusivity and sediment porosity. In the discussion, modifications are suggested for application of the results to remote infrared sensing.

2. Observations

2.1. Sites

[6] Observations span approximately one year (summer 2008 to summer 2009, although not all continuous) from two distinct tidal flats in Washington State, USA, which are shown in Figure 1. At the predominantly sandy flats at mouth of the Skagit River (approx. N 48.36°, W 122.50°), a total of 17 sites were occupied for a minimum of 10 days each (average 75 days). At the predominantly muddy flats at the southern end of Willapa Bay (approx. N 46.39°, W 123.97°), a total of 6 sites were occupied for a minimum of 10 days each (average 12 days). Both flats have regions of con-

[1]Applied Physics Laboratory, University of Washington, Seattle, Washington, USA.

0148-0227/10/2009JC005968

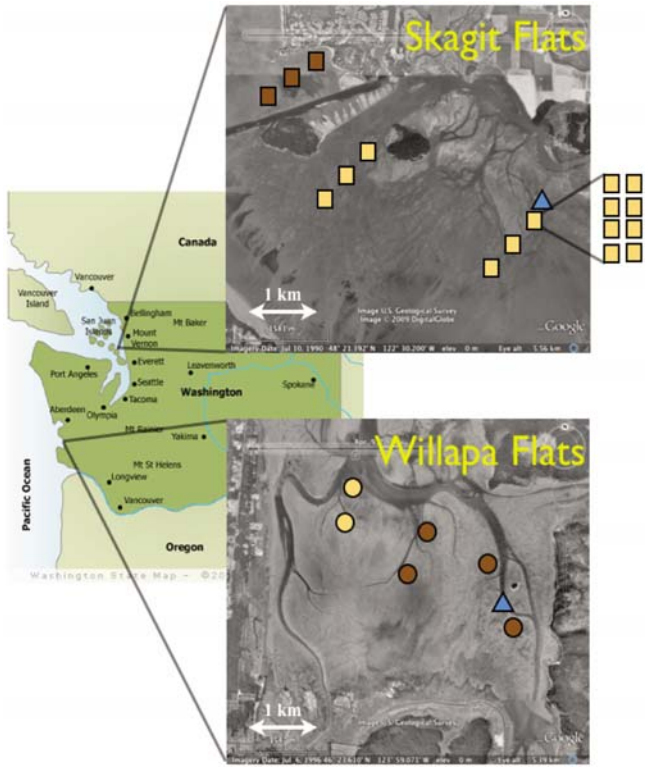

Figure 1. Locations of field observations and qualitative sediment classifications at the Skagit tidal flats (N 48.36°, W 122.50°) and the Willapa tidal flats (N 46.39°, W 123.97°) in Washington State, USA. Dots indicate temperature profile locations, and triangles indicate meteorological stations. Light colors are sandy locations and dark colors are muddy locations. The satellite images for the tidal flats are exported from Google Earth. Google Earth imagery© Google Inc. Used with permission. Note that at the Skagit flats, a subarray of eight instruments was deployed near the met station.

trasting composition (muddy or sandy, respectively), and sites for observation were chosen to span these contrasts. Sediment types at each point of observation are indicated in Figure 1, where sandy sites are characterized in field by the presence of bed forms (ripples) and easy walking compared with muddy sites that are characterized by smooth features and difficult walking. Observations span elevations from −0.5 m to +1.5 m, relative to mean lower low water, and the maximum tidal range at both sites is 4 m.

2.2. Temperature Profiles

[7] Time series of sediment temperature profiles were collected at each site using buried HOBO Temp Pro v2 loggers (Onset Computers, Bourne, MA). The loggers were affixed to metal sand anchors and spaced 10 cm in the vertical down to 50 cm burial depth. At the sediment surface, HOBO U20 water level loggers were used to record inundation and exposure times. The loggers sampled temperature at 5 minute intervals, which was chosen based on the measured response time of the instruments. Examples of the times series of sediment temperature profiles are shown in Figures 2e and 2f for sandy and muddy sites, respectively, where surface (z = 0 cm) temperatures increase dramatically during daylight low tides and the signal diffuses down to lower layers.

[8] The emplacement of the sand anchors caused a slight disturbance to the sediments, however the seabed was observed to recover after a single tidal cycle. Moreover, a random series of 100 test profiles using a Thomas Traceable RTD Platinum Thermometer No. 1235C87 (accuracy 0.1%) were consistent with logger observations to within the stated 0.2°C accuracy of the HOBO logger. Concerns over thermal conduction by the metal sand anchors were also addressed using data from the realtime probe, as well as during extensive laboratory testing (72 profiles using a heat lamp to simulate solar forcing of laboratory sediments).

2.3. Meteorological Forcing

[9] Meteorological data were collected using HOBO U30 weather stations (Onset Computers, Bourne, MA) at the locations shown in Figure 1. Data include: solar radiation, wind speed, wind direction, air temp, and relative humidity. Observations are recorded every 5 minutes (to match the sediment temperature profiles). At the Skagit tidal flats, the weather station was mounted on a 1.5 m tripod anchored to the top of Craft Island (28 m elevation), a rocky outcrop at the onshore edge of the flats. At the Willapa tidal flats, the weather station was mounted on a preexisting piling (7 m elevation) near Round Island, on the western edge of the Bear River Channel. Nearby stations from the Washington State University AgNet program are used to supplement these data during several short data gaps. AgNet observations are recorded every 15 minutes, and a nearest-neighbor interpolation scheme is used to create 5 min samples for use with the rest of the data set.

2.4. Sediment Sampling

[10] Ground truth samples of surface sediments were collected at each location, and sediment surface strength was measured in situ using a strain gage penetrometer (Forestry Suppliers Nos. 77114, 77116). The samples, approximately 10 cm^3 each, were sieved and then dry weights were used to determine percentages of sand and mud. For most sites, at least two samples were collected during different times (i.e., at the beginning and end of deployments). The composition did not change qualitatively between visits to any of the sites over the year, and duplicate sediment samples are all in close agreement. Porosity is not measured directly, because of difficulty retaining all of the pore water during sample collection. Instead, the percent of sand and mud is used to inferred porosity from an empirical relation following the onCALCULATION method used in dbSEABED by U.S. Geological Survey (http://pubs.usgs.gov/ds/2005/118/htmldocs/onCALCULATION.htm).

3. Methods

3.1. Surface Heat Budget

[11] The net heat input to sediments during low tide is estimated following *Kim et al.* [2007, and references therein] as

$$Q_{net} = Q_s - (Q_l + Q_e + Q_h), \quad (1)$$

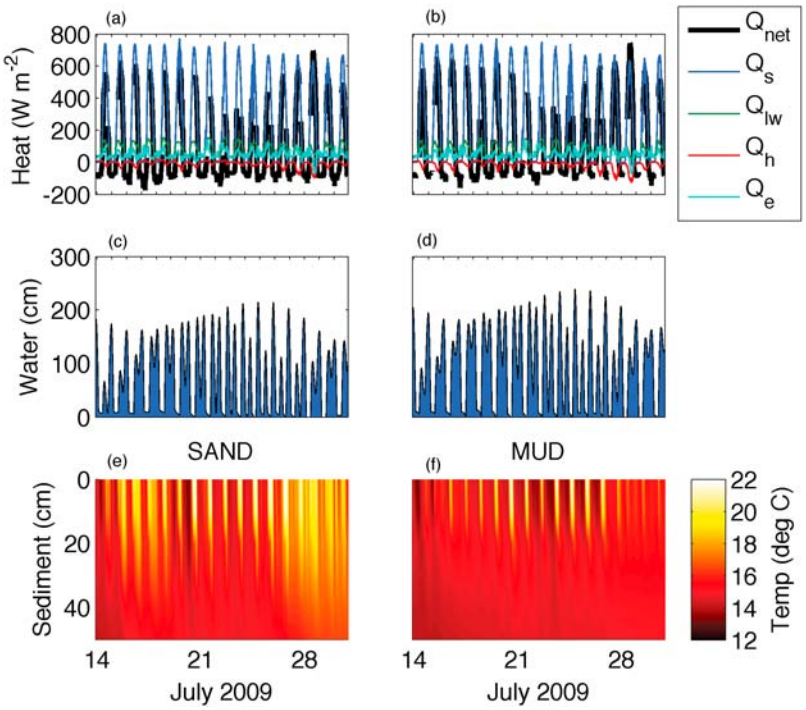

Figure 2. Example fortnight long time series of (a and b) heat fluxes, (c and d) tide level, and (e and f) vertical sediment temperature profiles from a sandy site (Figures 2a, 2c, and 2e) and a muddy site (Figures 2b, 2d, and 2f) in Skagit Bay. Sediment temperatures are predominately controlled by the uptake of heat during low tide exposure, as shown by Q_{net}, and that heat is subsequently diffused down to lower layers. The sandy site, which is at an elevation of −0.5 m ref. MLLW, has active heating down to 40 cm within the sediment. The muddy site, which is at an elevation of −0.6 m ref. MLLW, has active heating down to 20 cm within the sediment.

where Q_s is solar radiation, Q_l is long-wave radiative heat lost, Q_e is latent heat lost to evaporation, and Q_h is sensible heat lost (or gained) to the air. Although *Kim et al.* [2007] showed that tidal flat albedos range from 0.1 to 0.3 depending on water content, solar angle, and atmospheric transmittance, the incoming solar radiation Q_{so} is adjusted for reflection using a constant albedo of 0.2, such that $Q_s = 0.8Q_{so}$. Analysis is restricted to cloudless sky conditions, and thus long-wave downwelling radiation from clouds is neglected.

[12] Examples of the different terms in the surface heat budget are shown in Figures 2a and 2b for sandy and muddy sites, respectively, where Q_s dominates the other terms during midday low tides. Net heat fluxes of 500 W m^2 are common, and can be as high as 800 W m^{-2} during summer months.

3.2. Vertical Heat Budget

[13] Assuming a one-dimensional vertical balance, the net heat input at the surface of exposed sediments either is used to heat the immediate layer, according to its heat capacity, C, or is conducted down to a lower layer, according to its thermal conductivity, λ. Using a volumetric heat capacity C_v, the total heat budget is expressed as

$$Q_{net} = C_v \frac{dT}{dt} dz + \lambda \frac{dT}{dz}. \tag{2}$$

[14] At any internal (buried) layer, the input of heat at the remote boundary can be neglected, and a simple diffusion equation is expressed as

$$\frac{dT}{dt} = \kappa \frac{d^2T}{dz^2} + \epsilon, \tag{3}$$

where $\kappa = \frac{\lambda}{C_v}$ is the thermal diffusivity and ϵ is the error. Figure 3 shows examples of the data fit to this balance at a layer 20 cm below the surface, using the sandy and muddy sites from Figure 2. Other locations and layers are similar. The errors ϵ are shown by the scatter in Figure 3, and are likely related to horizontal terms excluded in the balance. In practice, this fit is calculated at each layer depth (10, 20, 30, and 40 cm) and then an average is taken to determine κ for a particular location. In addition to these observations and the work of *Kim et al.* [2007], several other studies have successfully observed thermal diffusion in tidal flat and marine sediments, including *Harrison* [1985], *Vugts and Zimmerman* [1985], *Harrison and Phizacklea* [1985], *Piccolo et al.* [1993], and *Wheatcroft et al.* [2007].

[15] The quality of the fit to the data, and thus the quality of the κ estimate for a given location, is quantified by the ratio of the observed $\frac{dT}{dt}$ variance to the mean-square error in the fit, and is referred to as the percent of observed variance explained by the vertical heat budget

$$VE(\%) = 100\left(1 - \frac{\langle \epsilon^2 \rangle}{\mathrm{var}\left(\frac{dT}{dt}\right)}\right). \tag{4}$$

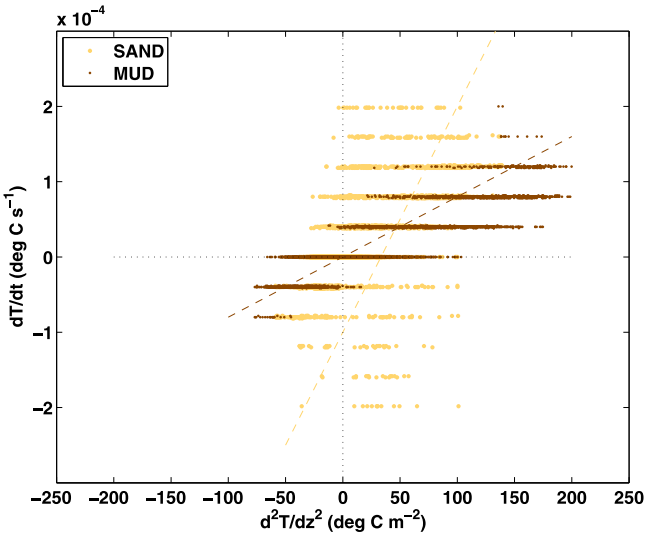

Figure 3. Examples of vertical diffusion of heat 20 cm below the surface for a sandy site (light color) and a muddy site (dark color) on the Skagit flats. Diffusivities are obtained via least-squares fitting of these data, and generally show higher diffusivities (i.e., steeper slopes of the fitted line) at sandy sites, compared with muddy sites. In this example, correlations are $r^2 = 0.71$ for sand and $r^2 = 0.84$ for mud, as determined from MATLAB's corrcoef routine using 7258 observed points. These are the same data as Figure 2.

The resulting estimate of diffusivity is compared with direct measurements of sediment composition and surface strength, as well as a theoretical model for the sediment porosity.

3.3. Theoretical Model for Sediment Porosity

[16] The amount of water in a given volume of saturated marine sediment is quantified by the porosity, n, as the ratio of water volume to total volume. A model for the thermal diffusivity of saturated sediment as a function of porosity, n, is formulated using the *Lovell* [1985] model for conductivity and the *Campbell and Norman* [1998] model for volumetric heat capacity as

$$\kappa = \frac{\lambda}{C_v} = \frac{\lambda_f^n + \lambda_s^{(1-n)} + 1}{\rho_f c_f n + \rho_s c_s (1-n)}, \qquad (5)$$

where λ_f and λ_s are the conductivities of the fluid and solid constituents, respectively, and c_f and c_s and the capacities of the fluid and solid constituents, respectively. Values of $\lambda_f = 0.6$ W m^{-1} K^{-1} and $c_f = 4.2$ kJ kg^{-1} K^{-1}, based on fresh water, are used throughout the analysis. Differences in the values of λ_f and c_f resulting from changes in salinity are negligible. Values of $\lambda_s = 8.6$ W m^{-1} K^{-1} and $c_s = 0.8$ kJ kg^{-1} K^{-1}, based on the standard properties for quartz minerals, are considered constant throughout this analysis. Using more specific estimates for λ_s and C_v does not change results appreciably, because, to first order, the dramatic difference between the λ_f and c_f values for water and the λ_s and c_s values for any solid mineral is what controls equation (5), not the absolute values of λ_s and c_s. More specifically, it is the difference in heat capacity between water and a solid mineral that dominates equation (5). The assumption that intertidal sediments are saturated with water during low-tide exposure is qualitatively confirmed at all observation locations by visual inspection. The persistence of saturation, even in sandy sediments, is possibly related to groundwater in the near proximity of a river mouth. However, it should be noted that the impact of drying, and related air infiltration to sediment pore space, is not included in equation (5).

[17] To relate inferred porosity to sediment samples collected in the field, an empirical result of $n = (0.4(100 - S) + 43)/100$ is used, where S is percent sand (http://pubs.usgs.gov/ds/2005/118/htmldocs/onCALCULATION.htm). The percent sand is determined from dried weights after sieving the samples to remove silt and clay particles. Although the use of a bulk relation between percent sand and porosity has large uncertainties, this method gives more consistent results than comparing wet and dry weights of the samples. A resistivity probe for in situ porosity estimates was not available.

4. Results

[18] The examples in Figure 2 show clearly the response of intertidal sediments to solar forcing, and Figure 3 shows the vertical diffusion of this forcing down to lower layers. In these examples, sandy sediments uptake heat rapidly, achieving much higher temperatures and deeper penetration of heat, compared with muddy sediments. Quantitatively, fitting these data to equation (3) results in diffusivities, κ, which are as much as twice as high for sand as for mud. Overall, the vertical heat balance (equation (3)) explains 76% of the observed variance averaged over all locations, and up to 97% at some locations (equation (4)). Figure 4 shows correlations between the diffusivity estimate and direct measurements of sediment composition and surface strength. The sandy sediments are effective at diffusing heat, and are clearly grouped apart from the muddy sediments which are about half as effective at diffusing heat. Likewise, elevated surface strengths are associated with increased thermal diffusivity because the sediments are more closely packed. Strength, however, is a complicated multivariate property of intertidal sediments, and there is no expectation that thermal diffusivity would be more than partially covariant.

[19] Figure 5 shows agreement between theoretical thermal diffusivity (equation (5)) and observed thermal diffusivity (equation (3)) as functions of porosity. The theoretical diffusivity is equivalent, to within 95% confidence, with a logarithmic regression of the observed diffusivity. The grouping is consistent between the Skagit and Willapa flats, despite large differences in the formation and evolution of these two flats. Thus, thermal properties alone are sufficient to distinguish between sandy and muddy intertidal sediments.

5. Discussion

[20] There is considerable scatter in the thermal diffusivities, which is likely owing to processes not described by the vertical balance. For example, horizontal heat transfers and advection by pore water may be important at some loca-

tions, such as near channel banks and other topographic features. In addition, sandy sediments may become dry enough during long periods of exposure that the saturation assumption is no longer valid. This is consistent with the larger scatter in sand observations, compared with mud observation, in Figure 3. In these cases, including air as a third component in equation (5) would potentially improve the fit, at the expense of solving for another variable (i.e., dry porosity). Biologic effects, such as albedo alteration by algal mats or ventilation by bioturbation, may be substantial at some locations.

[21] There are considerable variations in sediment profiles at small vertical scales that are not captured by these coarse (dz = 10 cm) observations [*Wheatcroft et al.*, 2007]. The focus of this work, however, is to quantify the bulk parameters of the upper 50 cm of intertidal sediments and verify a physical model relating thermal properties to geotechnical classification. As shown in Figure 2, 50 cm is the limit for thermal activity on tidal timescales. In addition, it is the bulk properties of the upper 50 cm determine the trafficability of intertidal flats, a critical operational parameter.

[22] Although there is scatter in the results, the basic classification of sandy and muddy sediments via physical modeling of thermal observations is successful. In a future paper, infrared remote sensing observations coincident with the data presented here will be used to map sediment type from scales of meters to kilometers. The infrared observations were collected from a small plane during several low tide exposures lasting a few hours each. Only surface temperatures are available from the remote observations, and thus further approximation to the balance in equation (2) will be required. One approach will be to empirically determine porosity as a function of an absorption coefficient β, related to the heating rate at the surface by $Q_{net} = \beta \frac{dT}{dt}$. Embedded in β is an assumption of a thin active layer at the surface with some nominal thickness dz that can be uniformly applied, and that any further diffusion can be neglected on short time scales.

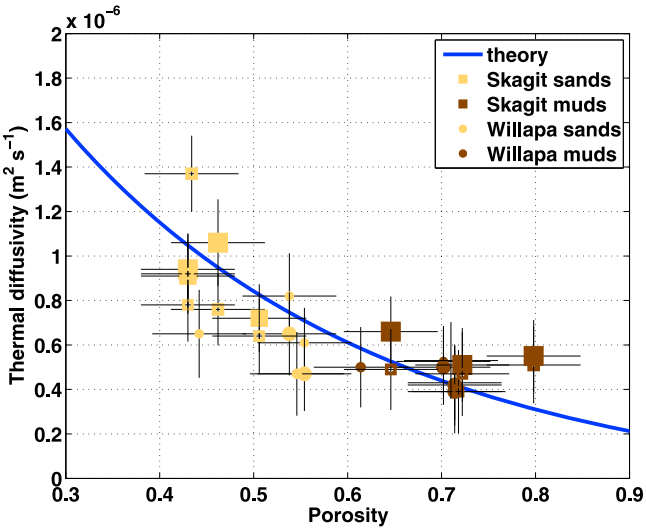

Figure 5. Theoretical (solid curve, equation (5)) and observed (symbols, equation (3)) thermal diffusivity as a function of sediment porosity. Squares are from Skagit sites and circles are from Willapa sites, and each symbol is scaled by the length of deployment (from 10 to 365 days). Uncertainties in diffusivity, shown by thin vertical lines, are the residual error in fitting the data to equation (3). Uncertainties in porosity, shown by thin horizontal lines, are the known error in estimating porosity from composition. The correlation between the theoretical diffusivity and the estimated diffusivity is r^2 = 0.78, which is significant at the 95% confidence level.

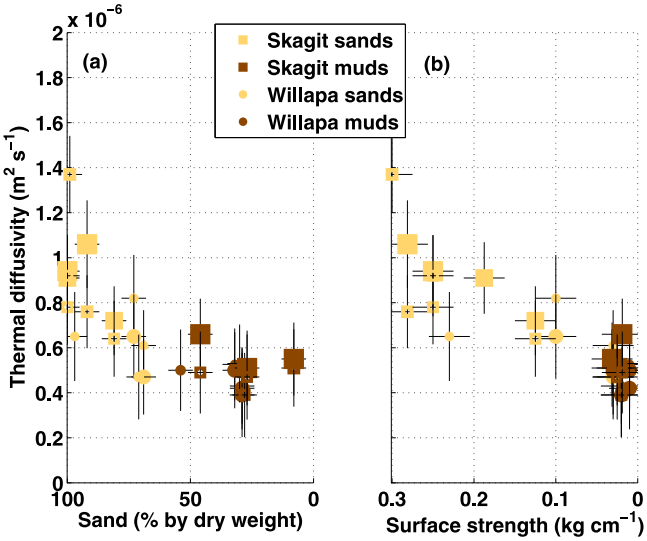

Figure 4. Thermal diffusivity as a function of (a) percent sand and (b) surface strength. Squares are from Skagit sites and circles are from Willapa sites, and each symbol is scaled by the length of deployment (from 10 to 365 days). Uncertainties in diffusivity, shown by thin vertical lines, are the residual error in fitting the data to equation (3). Uncertainties in sediment properties, shown by thin horizontal lines, are one standard deviation from repeat measurements at each location. The correlation between percent sand and diffusivity is r^2 = 0.75, and the correlation between strength and diffusivity is r^2 = 0.86. Both are significant at the 95% level.

[23] **Acknowledgments.** Thanks to A. de Klerk for designing, building, and testing the sediment temperature profilers. Thanks collaborators and field crews from the University of Washington for help deploying and recovering the temperature profilers, including: A. de Klerk, A. Ogston, C. Nittrouer, K. Lee, R. Hale, T. Drexler, C. Chickadel, J.P. Rinehimer, J. Talbert, and D. Polland. Supplemental solar radiation data provided by AgNet stations from Washington State University. Infrared data for proposal preparation provide by A. Jessup and C. Chickadel. Funding provided by a Young Investigator Program award from the Office of Naval Research (N000140710768).

References

Campbell, G. S., and J. M. Norman (1998), *An Introduction to Environmental Biophysics*, Springer, New York.

Cho, Y. K., T. W. Kim, K. W. You, L. H. Park, H. T. Moon, S. H. Lee, and Y. H. Youn (2005), Temporal and spatial variabilities in the sediment temperature on the Baeksu tidal flat, Korea, *Estuarine Coastal Shelf Sci.*, *36*, 302–308.

Guarini, J. M., G. Blanchard, P. Gros, and S. J. Harrison (1997), Modeling the mud surface temperature on intertidal flats to investigate the spatio-temporal dynamics of the benthic microalgal photosynthetic capacity, *Mar. Ecol. Prog. Ser.*, *153*, 25–36.

Harrison, S. J. (1985), Heat exchange in muddy intertidal sediments, Chichester Harbour, west Sussex, England, *Estuarine Coastal Shelf Sci.*, *20*, 477–490.

Harrison, S. J., and A. P. Phizacklea (1985), Seasonal changes in heat flux and heat storage in the intertidal mudflats of the forth estuary, Scotland, *J. Climatol.*, *5*, 472–485.

Jackson, D. R., and M. D. Richardson (2002), Seasonal temperature gradients within a sandy seafloor: Implications for acoustic propagation and scattering, *IEEE J. Oceanic Eng.*, *27*, 546–560.

Kim, T.-W., Y.-K. Cho, and E. P. Dever (2007), An evaluation of the thermal properties and albedo of a macrotidal flat, *J. Geophys. Res.*, *112*, C12009, doi:10.1029/2006JC004015.

Kim, T.-W., S. Kim, J. Choi, and J. Choe (2009), Angkor wat on the intertidal mudflats: Towers built by the manicure crab cleistostoma dilatatum (de haan) for thermo-regulated ventilation, *Integr. Comp. Biol.*, *49*(E91), 80.2.

Lovell, M. A. (1985), Thermal conductivity and permeability assessment by electrical resistivity measurements in marine sediments, *Mar. Geotech.*, *6*, 205–240.

Piccolo, M. C., G. M. E. Perillo, and G. R. Daborn (1993), Soil temperature variations on a tidal flat in Minas basin, Bay of Fundy, Canada, *Estuarine Coastal Shelf Sci.*, *35*, 345–357.

Subramaniam, D., and G. V. Frisk (1992), Seasonal variations of the sediment compressional wave-speed profile in the Gulf of Mexico, *J. Acoust. Soc. Am.*, *91*, 127–135.

Vugts, H. F., and J. T. F. Zimmerman (1985), Heat balance of a tidal flat area, Netherlands, *J. Sea Res.*, *19*, 1–14.

Wheatcroft, R. A., R. V. Johnson, and A. W. Stevens (2007), In situ time-series measurements of sub-seafloor sediment properties, *IEEE J. Oceanic Eng.*, *32*, 862–871.

J. Thomson, Applied Physics Laboratory, University of Washington, 1013 NE 40th St., Seattle, WA 98105, USA. (jthomson@apl.washington.edu)